Probing the Role of Sigma π Interaction and Energetics in the Catalytic Efficiency of Endo-1,4-β-Xylanase

Raushan Kumar Singh,[a] Manish Kumar Tiwari,[a] In-Won Kim,[a] Zhilei Chen,[b] and Jung-Kul Lee[a]

Department of Chemical Engineering, Konkuk University, Seoul, South Korea,[a] and Artie McFerrin Department of Chemical Engineering, Texas A&M University, College Station, Texas, USA[b]

Chaetomium globosum endo-1,4-β-xylanase (XylCg) is distinguished from other xylanases by its high turnover rate (1,860 s^{-1}), the highest ever reported for fungal xylanases. One conserved amino acid, W48, in the substrate binding pocket of wild-type XylCg was identified as an important residue affecting XylCg's catalytic efficiency.

Hemicellulose, which consists largely of xylan, is the second-most abundant component of plant cell walls, comprising approximately 33% of total dry weight plant biomass (11). Recently, microbial enzymes capable of depolymerizing xylan have been utilized for applications in the food, animal feed, and paper and pulp industries. These xylanases are characterized as group 10 and 11 glycoside hydrolases (GHs) based on their amino acid sequence homology, hydrophobic cluster, and three-dimensional (3-D) structures (6). Most glycosidase reactions involve two essential carboxyl residues: a proton donor and a nucleophile. The importance of the two completely conserved and catalytically important glutamate residues in the GH11 family has been previously demonstrated using site-directed mutagenesis (6, 16). Many biological processes rely on carbohydrate-protein interactions. In addition to their ability to form hydrogen bonds (H-bonds), a common feature of carbohydrate-binding proteins is the interaction between the α-face of the carbohydrate and the face of one of their aromatic side chains (4). Indole, phenol, and benzene (which are the side chains of tryptophan, tyrosine, and phenylalanine, respectively) are all electron-rich aromatic systems (5, 9). Because indole is electron rich and possesses an H-bond donor, it can engage in a variety of supramolecular interactions. These characteristics make the indole of tryptophan a unique chemical moiety in peptides and proteins (2). In this study, we cloned and characterized a novel xylanase, endo-1,4-β-xylanase (XylCg), from *Chaetomium globosum* CBS 148.51. This enzyme exhibits >12-fold-higher catalytic efficiency (7,640 ml s^{-1} mg^{-1}) than the most active fungal xylanase reported in the literature (597 ml s^{-1} mg^{-1}, for a xylanase from *Aspergillus awamori* CMI 142717; see Table S1 in the supplemental material). Using the crystal structure of *Trichoderma reesei* Xyl II as the template, we constructed a 3-D model of XylCg. Examination of the 3-D model of XylCg docked with xylohexaose revealed that residue W48 interacts with the pyranose ring of the carbohydrate substrate, suggesting that this residue may be essential for catalysis. We further characterized the role of W48 in the catalysis of XylCg.

An uncharacterized gene (*XylCg*, NCBI Gene accession number 4386742) thought to encode a xylanase was cloned from *C. globosum* into pET28(a), and its complete nucleotide sequence was determined. Subsequent DNA sequence analysis revealed an open reading frame of 660 bp, capable of encoding a polypeptide of 219 amino acid residues. To verify that *XylCg* is a xylanase gene, the recombinant plasmid pET 28(a)-*XylCg* was transformed into *Escherichia coli* BL21-CodonPlus (DE3)-RIL competent cells for

heterologous expression of the enzyme as an N-terminally His$_6$-tagged protein. A significantly higher level of xylanase activity was observed in the soluble *E. coli* lysate harboring pET 28(a)-*XylCg* than in the empty vector control lysate. The recombinant xylanase XylCg was purified to electrophoretic homogeneity from the culture supernatant using Ni-nitrilotriacetic acid (NTA) affinity chromatography. Analysis of the purified XylCg by SDS-PAGE revealed the protein to be more than 95% pure, with a denatured molecular mass of 24.6 kDa as determined using SDS-PAGE (see Fig. S1 in the supplemental material). Size exclusion chromatography on a Sephacryl S-300 high-resolution column resulted in the elution of a symmetrical peak of enzyme activity that corresponded to an M_r of approximately 25 kDa, suggesting that the recombinant XylCg is a monomeric enzyme.

The enzymatic activity of XylCg was measured at different temperatures (35°C to 65°C). The optimal temperature for xylanase activity was 40°C, which was only valid under the conditions used for measurement. The enzyme retained more than 90% of the maximum activity when assayed at 45°C, with more than 50% retained at 50°C and more than 40% at 55°C. The optimum pH was 5.5, and more than 80% of the maximum activity was retained between pH 5.0 and 7.0. Hydrolytic activity was observed with most xylans obtained from different sources, with a maximal value of 4,310 U mg protein^{-1} with oat spelt xylan. The enzyme activities using birch wood xylan, rice straw, avicel, and sugarcane bagasse as substrates were 52.8%, 24.3%, 21.6%, and 2.6%, respectively. No activity was detected with cellulose, carboxymethyl cellulose, *p*-nitrophenyl-β-D-glucopyranoside, or *p*-nitrophenyl-β-D-xylopyranoside. The initial rate of product formation was determined in the standard assay mixture at pH 5.5. Using oat spelt xylan as a substrate, hyperbolic saturation curves were obtained, and the corresponding double-reciprocal plots were linear. Under optimal assay conditions, the apparent V_{max} and K_m values of the purified wild-type XylCg were 4,530 U (mg pro-

tein)$^{-1}$ and 0.243 mg ml^{-1}, respectively. The catalytic efficiency (k_{cat}/K_m) was 7,640 ml s^{-1} mg^{-1}. This catalytic efficiency is >270-fold higher than that of xylanase isolated from *T. reesei* (see Table S1 in the supplemental material).

To further understand its high catalytic efficiency, the interactions of xylohexaose with the amino acid residues in the substrate binding pocket (SBP) of XylCg were compared with those in the template structure (*T. reesei* Xyl II). A 3-D model of XylCg was constructed using the crystal structure of *T. reesei* Xyl II as a template (see the supplemental material), and its overall structure was found to be similar to that of *T. reesei* Xyl II (see Fig. S2 and S3 in the supplemental material). According to the homology model, E115 and E206 are putative active-site residues of XylCg which correspond to E86 and E177, respectively, in *T. reesei* Xyl II (17). The substrate xylohexaose was docked into the homology model of XylCg and the template crystal structure of *T. reesei* Xyl II (PDB protein structure accession number 2DFB) by using DS 3.1 software (3). Xylohexaose docked into the SBP of Xyl II revealed an extended conformation with a distance of 3.4 Å between an anomeric carbon and nucleophile E86 (see Fig. S4 in the supplemental material). Xylohexaose interacted with Y73 and Y171 by H-bond only and with W18 by one H-bond and one sigma-π interaction. In the SBP of XylCg, however, xylohexaose formed H-bonds with Y106, Y117, and Y125 and one H-bond plus two sigma-π interactions with W48 (equivalent of W18 in Xyl II) (Fig. 1A). The presence of the additional H-bond and sigma-π interaction likely contributes to the reduced distance (3.1 Å) between the anomeric carbon and nucleophile E115 (3.4 Å in Xyl II), leading to higher stability of the enzyme-substrate complex, more efficient formation of productive complex, and accumulation of the glycosyl-enzyme intermediate. Additionally, the calculated binding energy of xylohexaose for XylCg (−52.3 kcal mol^{-1}) was lower than that for the template Xyl II (−46.1 kcal mol^{-1}), supporting the higher affinity of XylCg toward the substrate.

We analyzed the function of residues in the SBP of XylCg. This strategy involved (i) screening conserved residues by multiple sequence alignment, (ii) identifying conserved residues that contact the substrate by using molecular dynamics simulation, and (iii) individual site-directed mutagenesis to alter these specific residues. Conserved residues were identified by sequence alignment of XylCg with other xylanases. The overall similarity among the six xylanase sequences from different fungal strains (*Aspergillus versicolor*, *Aspergillus niger*, *Trichoderma* sp. strain SY, *T. reesei*, and *C. globosum*) was 22.6%. A conserved domain search (RPSBLAST) analysis confirmed the presence of conserved catalytic residues (E115 and E206) and a PSIXG consensus sequence of the GH11 family (Fig. 2). Residues E115 and E206 are located in the middle of a pocket formed by a twisted region of the β-strand (β8 and β13) and may function as the nucleophile and the acid/base catalyst, respectively. Glutamic acid residues at these positions are strictly conserved among all GH sequences. The thumb tip sequence of PSIXG is also highly conserved among the GH11 xylanases (8, 10).

Thirty-one amino acid residues, including the 2 active-site residues, were found within the 5-Å cylindrical tunnel of the SBP of XylCg. Of the 31 residues, 15 were conserved between XylCg and Xyl II, including the putative catalytic residues, E115 and E206 (corresponding to E86 and E177, respectively, in *T. reesei* Xyl II; see Fig. S5 in the supplemental material). E86 and E177 in *T. reesei* Xyl II function as the nucleophile and the proton donor/receptor,
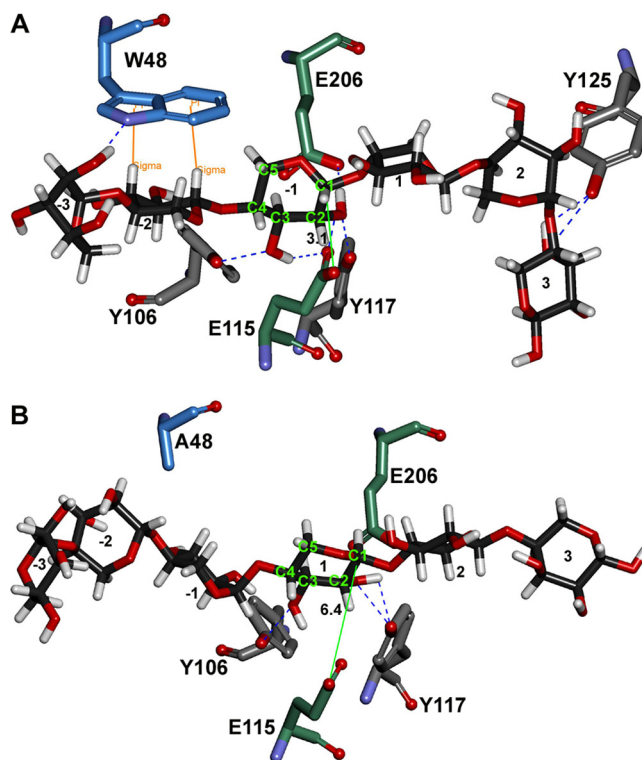

FIG 1 Homology model of the XylCg active site with bound xylohexaose substrate. (A) Xylohexaose was docked into the substrate binding pocket of wild-type XylCg. The intermolecular distances are the results of modeling. Catalytic residues are indicated in light green. (B) Model of the W48A mutant's active site with bound xylohexaose substrate. Xylohexaose was docked into the substrate binding pocket of the W48A mutant. The intermolecular distances are the results of modeling. Catalytic residues are indicated in light green. Hydrogen bonds and sigma-π interactions are represented with blue dashed lines and orange lines, respectively. Distances between anomeric carbon and nucleophile (E115) are represented in angstroms with green lines.

respectively (17). When xylohexaose was docked into the SBP of wild-type XylCg, the hydroxyl groups of C-2 and C-1 of the pyranose ring formed H-bonds (2.0 Å and 2.4 Å) with oxygen atoms in the carboxyl groups of the active-site residues E115 and E206, respectively (Fig. 1A). Additionally, the carboxyl group of E115 aligned well with the −1 anomeric carbon atom (3.1 Å) in a position consistent with its role in nucleophilic attack. To confirm enzymatic activity of E115 and E206 in XylCg, site-directed mutagenesis was performed to change these two residues to Ala. The mutant XylCg with E115A or E206A showed no measurable xylanase activity, confirming that these residues are required for the hydrolysis reaction. We next determined the contribution of the other 13 conserved residues within the 5-Å cylindrical tunnel in the SBP of XylCg (Fig. 3). Y102, Y106, W108, Y125, and W167 were previously identified as critical for substrate binding and hydrolysis through crystallographic and mutagenesis studies (7, 12, 13, 14, 15). N74 is important for activity at the optimal pH, and I157 is involved in product release from the active site (1, 8). Thus, we examined the roles of the remaining six residues (W48, Y117, S129, R151, P155, and Y208) by alanine scanning. Alanine-substituted enzymes were expressed and purified, and their activities toward oat spelt xylan were compared (data not shown). Substitution at W48 significantly decreased xylanase activity. The spe-

FIG 2 Multiple sequence alignment and secondary structure prediction comparing family 11 xylanases of *Aspergillus versicolor*, *Aspergillus niger*, *Trichoderma* sp. SY, and *Trichoderma reesei* with XylCg of *C. globosum*. Conserved amino acids are indicated with a blue background. Catalytic residues and W48 are indicated with yellow and red backgrounds, respectively. A consensus sequence (PSIXG) of the GH11 family is represented within the red box. Blue arrows and orange bars represent beta sheets and alpha helices, respectively.

cific activity of the W48A mutant was 121 U mg protein^{-1} for oat spelt xylan, corresponding to 2.8% of the activity of the wild-type enzyme (4,310 U mg protein^{-1}), suggesting that W48 may play an important role in XylCg's catalytic activity.
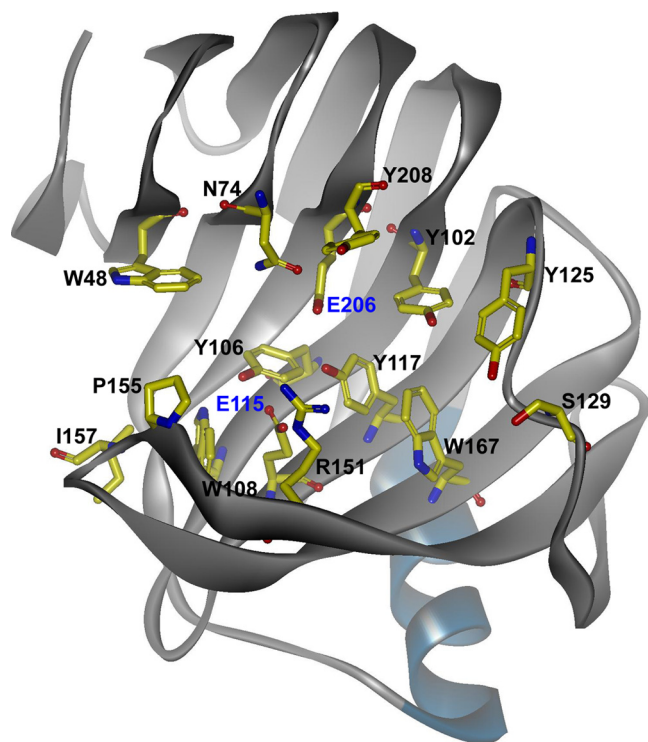

FIG 3 Molecular modeling of the XylCg active-site pocket. The catalytic domain of XylCg model showing conserved residues is represented as a stick model. The two catalytic residues (E115 and E206) are labeled in blue. This figure was generated using DS 3.1.

Trp in position 48 was replaced with aliphatic or aromatic residues using site-directed mutagenesis. All mutants were expressed at levels similar to the expression of the wild type. Purified proteins of the wild type and with W48Y and W48A mutations exhibited similar CD spectra, with ellipticity minima of comparable amplitude in a range of 220 to 230 nm (see Fig. S6 in the supplemental material). Little or no conversion of oat spelt xylan was observed for W48 variants containing aliphatic amino acids (W48R, W48N, W48D, W48C, W48I, W48L, and W48V), regardless of the polarity and charge. This is probably due to the disruption of H-bonding and sigma-π interactions between the substrate and residue at position 48, resulting in an improper orientation for nucleophilic attack by the carboxyl group of E115 in the active site. However, variants with W48 replaced by aromatic amino acids (W48Y and W48F) retained significant activity toward oat spelt xylan. The specific activities of the W48Y and W48F mutants were 2,993 and 1,898 U mg protein^{-1}, which were 69% and 44% of the wild-type XylCg activity, respectively. Sequence alignments of 283 GHs from 27 different GH families revealed that position 48 was highly conserved with aromatic amino acids (W/Y/F). These results suggest that this position plays an important role in the catalytic reaction of all GHs.

Kinetic parameters were determined for W48Y, W48F, and W48A mutants using oat spelt xylan as a substrate. Changes in $\Delta(\Delta G)$ were determined on the basis of the kinetic parameters of the mutant enzymes (Table 1). Compared to wild-type XylCg, the W48Y and W48F mutants showed significant decreases in catalytic efficiency (1,650 and 619 ml s^{-1} mg^{-1}, respectively) and increases in $\Delta(\Delta G)$ values (3.97 and 6.2 kJ mol^{-1}, respectively). The Trp48-to-Tyr mutation resulted in only one sigma-π interaction between the pyranose ring and Tyr at position 48 (see Fig. S7 in the supplemental material). This interaction probably enabled proper orientation of the substrate, resulting in stabilization of the protein-ligand complex. In the case of the W48A mutant, docking

TABLE 1 Kinetic parameters determined for XylCg wild type and W48 mutants[a]

Enzyme variant	V_{max} (U mg protein^{-1})	K_m (mg ml^{-1})	k_{cat}[b] (s^{-1})	k_{cat}/K_m (ml s^{-1} mg^{-1})	$\Delta(\Delta G)$[c]
Wild type	4,530 ± 230	0.24 ± 0.02	1,860 ± 90	7,640 ± 1,000	0
W48Y	3,040 ± 156	0.75 ± 0.04	1,250 ± 60	1,650 ± 170	3.97
W48F	1,990 ± 90	1.32 ± 0.07	816 ± 38	619 ± 61	6.20
W48A	126 ± 7	9.30 ± 0.45	51.6 ± 2.4	5.5 ± 0.5	17.9

[a] The V_{max}, K_m, and k_{cat} values presented are means ± standard deviations.
[b] The k_{cat} values were calculated by considering the enzyme to be a monomeric form. Values are means ± standard deviations of results from three experiments.
[c] $\Delta(\Delta G) = -RT \cdot \ln[(k_{cat}/K_m)\text{mut}/(k_{cat}/K_m)\text{wt}]$, where (k_{cat}/K_m)mut and (k_{cat}/K_m)wt are the k_{cat}/K_m ratios for the mutant and the wild-type, respectively, R is the ideal gas constant, and T is the temperature in Kelvin.

showed no interaction between the pyranose ring of the substrate and the Ala (Fig. 1B). The disruption of H-bonding and the sigma-π interaction in the W48A mutant probably displaced xylohexaose in the active-site pocket. This displacement increased the distance between E115 and the −1 anomeric carbon to 6.4 Å, abolishing the catalysis reaction.

Isothermal titration calorimetry (ITC) was used to characterize the thermodynamics of XylCg and its variants upon binding to oat spelt xylan (see the supplemental material). The K_d (dissociation constant) and the binding enthalpy ΔH_a were determined for inactive mutants (XylCg [E115Q], XylCg [E115Q W48A], and XylCg [E115Q W48Y]), which lack the catalytic acid base residue to prevent significant hydrolysis of the substrate during the titration experiments. Representative thermograms for the titration of XylCg (E115Q), XylCg (E115Q W48A), and XylCg (E115Q W48Y) upon binding to oat spelt xylan are shown in Fig. 4A and B; also see Fig. S8 in the supplemental material. All the titration curves fit well into the independent binding model system with a calculated n (stoichiometry) of 1 ± 0.08 (mean ± standard deviation). The binding curves shown in the insets in Figure 4 indicate the heat evolved per mole of titrant as a function of the molar ratio of total ligand to total enzyme. The binding affinity of the substrate to XylCg (E115Q) ($K_d = 0.14$ μM) was 114-fold higher than that to XylCg (E115Q W48A) ($K_d = 24.4$ μM). Binding was driven by the energy contribution ΔG^a (Gibbs free energy) values of −41.1, −39.7, and −27.6 kJ mol^{-1} for the XylCg (E115Q), XylCg (E115Q W48Y), and XylCg (E115Q W48A) variants, respectively. Compared to the XylCg (E115Q) binding, XylCg (E115Q W48Y) and XylCg (E115Q W48A) binding to oat spelt xylan showed increases in ΔG^a of 1.40 and 13.5 kJ mol^{-1}, respectively. The slight increase in ΔG^a for XylCg (E115Q W48Y) is probably due to the absence of H-bonding between the residue at position 48 and the pyranose ring of xylohexaose (see Fig. S7 in the supplemental material). A significant increase in entropic penalty in the mutants was found to outweigh the enhanced enthalpic contribution. Thermodynamic parameters derived from the analyses are shown in Table 2. The heat capacity change at constant pressure ($\Delta C_p = \Delta H_a / \Delta T$, where ΔH_a and T are binding enthalpy and temperature, respectively) for the binding reaction was determined from data obtained at different temperatures. Plotting the ΔH_a of binding versus temperature for XylCg (E115Q) and its variants showed a linear correlation, indicating that the ΔC_p for binding is constant over the temperature range used (see Fig. S9 in the supplemental material). C_p values can be used as a reliable tool to evaluate the contribution of sigma-π interactions to the binding mechanism (18). The ΔC_p values for XylCg (E115Q), XylCg (E115Q W48Y), and XylCg (E115Q W48A) were −1,290, −1,090, and −726 J M^{-1} K^{-1}, respectively. The 564 J M^{-1} K^{-1} increase in ΔC_p for XylCg

(E115Q W48A) indicates a loss of the sigma-π interaction, which agrees with the proposed role of W48 in substrate binding of XylCg and in stabilizing the enzyme-substrate complex by H-bonding and sigma-π interactions.
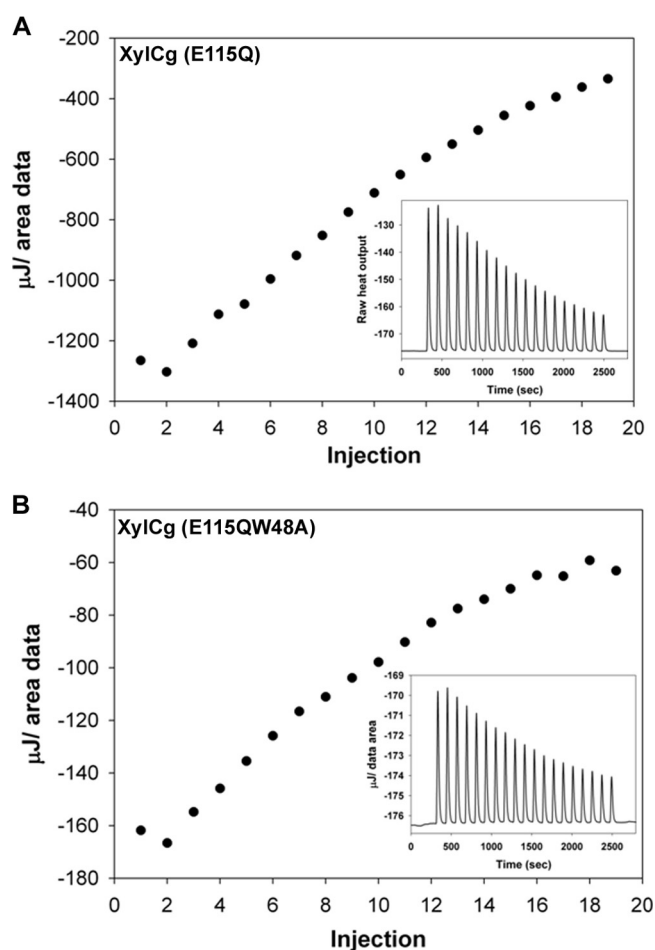

FIG 4 Thermodynamic contributions to oat spelt xylan binding by XylCg (E115Q) and its variants as determined by isothermal titration calorimetry. (A) An amount of 0.04 mg of purified XylCg (E115Q) was titrated with repeated additions of 2.5 μl of oat spelt xylan at 40°C. Calorimetric traces of heat released and enthalpic binding curves (insets) fitted with a one-site independent binding model are shown. (B) An amount of 0.03 mg of purified XylCg (E115Q W48A) mutant was titrated with repeated additions of 2.5 μl of oat spelt xylan at 40°C. The stoichiometry of the ratio was approximately 1 to 2 in all experiments (three independent titrations were performed for each protein). Gibbs free energy, ΔG^a, is calculated from $\Delta G^a = -RT \cdot \ln K$, where K is the equilibrium constant, R is the ideal gas constant, and T is the absolute temperature in Kelvin.

TABLE 2 Thermodynamic parameters determined by ITC for XylCg (E115Q) and W48 mutants[a]

Enzyme variant	$K_a \times 10^4$ (M^{-1})	K_d (μM)	ΔG^a	$\Delta(\Delta G^a)$	ΔC_p (J M^{-1} K^{-1})
XylCg (E115Q)	732	0.14	−41.1	0	−1,290
XylCg (E115Q W48Y)	427	0.23	−39.7	1.40	−1,090
XylCg (E115Q W48A)	4.10	24.4	−27.6	13.5	−726

[a] All energy parameters are represented in kJ mol^{-1}. ΔG^a, free binding energy. Log K, K_d, and ΔG^a are calculated using the mathematical relation $\Delta G^a = -RT \cdot \ln K$, where K is the equilibrium constant, R is the ideal gas constant, and T is the absolute temperature in Kelvin. Values of ΔC_p were derived from the slopes of the linear correlation of changes in the binding enthalpies (ΔH_a) at different temperatures.

Collectively, the present study reports the detailed characterization of a novel xylanase, XylCg, with the highest catalytic efficiency (7,640 ml s^{-1} mg^{-1}) ever reported for a fungal xylanase. Molecular modeling, substrate docking, and site-directed mutagenesis studies indicated that a conserved amino acid, W48, in the SBP plays an important role in the catalytic efficiency of XylCg. Molecular dynamics simulation and ITC studies confirmed that an aromatic amino acid at position 48 stabilizes the enzyme-substrate complex through H-bonding and sigma-π interactions between the pyranose ring of the sugar and the aromatic side chain of the residue at position 48. This work demonstrates the utility of XylCg for the enzymatic pretreatment of biomasses and should be helpful in understanding the catalysis of the GH family enzymes.

REFERENCES

1. **Andre-Leroux G, Berrin JG, Georis J, Arnaut F, Juge N.** 2008. Structure-based mutagenesis of *Penicillium griseofulvum* xylanase using computational design. Proteins **72**:1298–1307.
2. **Gokel GW.** 2007. Indole, the aromatic element of tryptophan, as a pi-donor and amphiphilic headgroup. Int. Congr. Ser. **1304**:1–14.
3. **Jommuengbout P, Pinitglang S, Kyu KL, Ratanakhanokchai K.** 2009. Substrate-binding site of family 11 xylanase from *Bacillus firmus* K-1 by molecular docking. Biosci. Biotechnol. Biochem. **73**:833–839.
4. **Laughrey ZR, Kiehna SE, Riemen AJ, Waters ML.** 2008. Carbohydrate-pi interactions: what are they worth. J. Am. Chem. Soc. **130**:14625–14633.
5. **Mecozzi S, APWJ, Dougherty DA.** 1996. Cation-pi interactions in simple aromatics: electrostatics provide a predictive tool. J. Am. Chem. Soc. **118**:2307–2308.
6. **Miao S, Ziser L, Aebersold R, Withers SG.** 1994. Identification of glutamic acid 78 as the active site nucleophile in *Bacillus subtilis* xylanase using electrospray tandem mass spectrometry. Biochemistry **33**:7027–7032.
7. **Pollet A, et al.** 2010. Mutagenesis and subsite mapping underpin the importance for substrate specificity of the aglycon subsites of glycoside hydrolase family 11 xylanases. Biochim. Biophys. Acta **1804**:977–985.
8. **Pollet A, et al.** 2009. Crystallographic and activity-based evidence for thumb flexibility and its relevance in glycoside hydrolase family 11 xylanases. Proteins **77**:395–403.
9. **Ryzhov V, RCD.** 1999. Interactions of phenol and indole with metal ions in the gas phase: models for tyr and trp side-chain binding. J. Am. Chem. Soc. **121**:2259–2268.
10. **Sapag A, et al.** 2002. The endoxylanases from family 11: computer analysis of protein sequences reveals important structural and phylogenetic relationships. J. Biotechnol. **95**:109–131.
11. **Sa-Pereira P, Paveia H, Costa-Ferreira M, Aires-Barros M.** 2003. A new look at xylanases: an overview of purification strategies. Mol. Biotechnol. **24**:257–281.
12. **Tahir TA, et al.** 2002. Specific characterization of substrate and inhibitor binding sites of a glycosyl hydrolase family 11 xylanase from *Aspergillus niger*. J. Biol. Chem. **277**:44035–44043.
13. **Torronen A, Rouvinen J.** 1995. Structural comparison of two major endo-1,4-xylanases from *Trichoderma reesei*. Biochemistry **34**:847–856.
14. **Vandermarliere E, et al.** 2008. Crystallographic analysis shows substrate binding at the −3 to +1 active-site subsites and at the surface of glycoside hydrolase family 11 endo-1,4-beta-xylanases. Biochem. J. **410**:71–79.
15. **Vardakou M, et al.** 2008. Understanding the structural basis for substrate and inhibitor recognition in eukaryotic GH11 xylanases. J. Mol. Biol. **375**:1293–1305.
16. **Wakarchuk WW, Campbell RL, Sung WL, Davoodi J, Yaguchi M.** 1994. Mutational and crystallographic analyses of the active site residues of the *Bacillus circulans* xylanase. Protein Sci. **3**:467–475.
17. **Watanabe N, Akiba T, Kanai R, Harata K.** 2006. Structure of an orthorhombic form of xylanase II from *Trichoderma reesei* and analysis of thermal displacement. Acta Crystallogr. D Biol. Crystallogr. **62**:784–792.
18. **Zolotnitsky G, et al.** 2004. Mapping glycoside hydrolase substrate subsites by isothermal titration calorimetry. Proc. Natl. Acad. Sci. U. S. A. **101**:11275–11280.